

Preprint
To be submitted:
ICAVS Special Issue
Vibrational Spectroscopy

Chemical Imaging of Thin Film Polymer Blends With Near-Field Infrared Microscopy and Spectroscopy

Stephan J. Stranick¹, Xiaohong Gu¹, D. Bruce Chase² and Chris A. Michaels^{1,*}

¹*National Institute of Standards and Technology, Gaithersburg, MD 20899 USA*

²*DuPont Central Research and Development, Wilmington, DE 19880 USA*

*Corresponding Author: Tel: (301) 975-5418, Fax: (301) 926-6689

email address: chris.michaels@nist.gov

Keywords: Chemical Imaging, NSOM, Near-Field Microscopy, Infrared Spectroscopy, Infrared Microscopy, Polymer Blends

Abstract

The utility of an infrared scanning near-field microscope in the characterization of the mesoscale structure of thin film polymer blends is demonstrated. This unique IR microscope couples the nanoscale spatial resolution of scanning probe microscopy with the chemical specificity of vibrational spectroscopy. This powerful combination allows the *in situ* mapping of chemical functional groups with subwavelength spatial resolution. Key features of this instrument include broad tunability and bandwidth, parallel spectral detection for high image acquisition rates and IR transparent, near-field, aperture probes. Near-field spectral images of a thin film of polystyrene/poly (ethyl acrylate) acquired in the C-H stretching region are used to benchmark the chemical imaging capabilities of this microscope. Analysis of the near-field infrared spectra yields information about the nanoscale chemical morphology of this sample that is consistent with results from previous chemical modification/AFM studies. Finally, the relative contributions of scattering and absorption to the overall near-field transmission (extinction) contrast in these images are discussed.

Introduction

The ability to chemically characterize heterogeneous systems on the nanometer scale continues to grow in importance and to impact key applications in the fields of materials science (phase segregated systems), nanotechnology (molecular electronics), and catalysis (single site catalysts). Detailed information on this length scale is necessary to test and evaluate advanced materials and is critical to their continued development. A promising strategy for the development of a non-destructive, nanometer scale chemical microscopy involves coupling the high spatial resolution of a proximal probe microscope with the chemical specificity of molecular spectroscopy. Molecular spectroscopies can provide remarkably detailed descriptions

of elementary chemical processes such as the dynamics of bond making and bond breaking. However, they are generally restricted to length scales governed by the asymptotic nature of light: spatial confinement of the source radiation is limited to approximately one half the wavelength. This often limits the application of these techniques to homogenous sample systems or systems where the regions of interest are sufficiently dilute. Proximal probe microscopies such as scanning tunneling microscopy and atomic force microscopy (AFM) provide researchers with the ability to view sample surfaces on the atomic scale. Generally scanned probe microscopes are not capable of revealing the identity of the atoms and molecules that comprise the sample under study. Thus a tool that performs measurements on complex, heterogeneous, nanometer scale systems with the same exacting level of chemical detail that conventional spectroscopic techniques currently provide on macroscopic sample systems remains elusive.

In 1928, Synge recognized that the resolution limit of conventional optics could be circumvented by illuminating the sample through an aperture that was significantly smaller than the wavelength of light, while keeping the sample-to-aperture separation fixed at a distance that was also much smaller than the wavelength of light: a region referred to as the optical near-field. [1] In Synge's scheme, the resolution obtained is a function of the aperture size and its distance from the sample and is no longer governed by diffractive effects. The first demonstrations of near-field scanning optical microscopy (NSOM) in this experimental form were carried out by research groups headed by Pohl [2] at IBM Zurich and Lewis [3] at Cornell University. One of the many variations of NSOM involves illumination of a sample through a nanometer scale aperture that is placed at the end of an optical waveguide (optical fiber) while controlling the sample-to-aperture separation using shear-force feedback. [4,5] This precise positional control and high spatial confinement of the electromagnetic fields enables one to couple the chemical

specificity of vibrational spectroscopy with the nanometer scale resolution of a proximal probe microscope.

With the advent of intense laser sources and novel methods for generating small optical apertures, inroads have been made in the coupling of near-field optical methods with spectroscopy. Several research groups have developed techniques that combine conventional spectroscopies with NSOM. Contrast mechanisms that rely on vibrational spectroscopy (infrared absorption [6-14] and Raman [15-22] spectroscopies), dielectric spectroscopy (microwave dispersion), [23-27] and non-linear spectroscopy [28-30] have all been demonstrated at length scales below the diffraction limit of light. In this present study, we demonstrate the application of broadband, near-field infrared spectroscopy and microscopy as a tool for the characterization of spatial variations in chemical composition in a thin film polystyrene/poly(ethyl acrylate) (PS/PEA) blend. Information about the chemical morphology of this sample is derived from near-field IR transmission images and spectra and is compared to results from previous chemical modification/AFM studies. [31] Finally, the interplay of absorption and scattering effects in the determination of the near-field transmission (extinction) image contrast is also discussed.

Experimental

Illumination mode NSOM, in which an aperture probe is used as a subwavelength light source, was utilized in this work. This light source was fabricated by tapering and metal coating an IR transmitting, single mode optical fiber. Next, IR radiation is brought incident to the aperture by coupling light from a broadband, tunable laser into the optical fiber. The transmitted near-field radiation is then collected and collimated by the IR compatible optics of a conventional far-field microscope. After collimation, the scattered radiation (sample beam), along with a reference beam from the IR light source, is steered into an infrared focal plane array

based spectrometer. Collection of spectral images (parallel collection of spectra at each (x,y) scan point) with this scheme requires only a single sample scan, resulting in both fast data acquisition times and robust spectroscopic measurements. The elements of this infrared microscope have been described in considerable detail elsewhere, [12] but are briefly outlined here for completeness.

The illumination mode near-field probes are fabricated from single mode, fluoride glass optical fibers. The etching methodology is similar to that used in the fabrication of NSOM tips from glass [32,33] and chalcogenide [34] fibers. The broadband infrared light source is based on a commercial system that includes a Ti:sapphire oscillator and 250 kHz regenerative amplifier that pumps a beta-BaB₂O₄ optical parametric amplifier (OPA). Mid-infrared light is generated by difference frequency mixing the near-infrared signal and idler beams from the OPA in a 1-mm thick AgGaS₂ crystal, cut for type-I mixing. This difference frequency generation scheme has a demonstrated tuning range of 2.5 μm to 12 μm . [35] Typical average powers at 3.6 μm range from 8 mW to 12 mW with an optimized spectral FWHM of approximately 150 cm^{-1} . The small fraction of light transmitted through the sub-wavelength aperture (1 to 5 $\times 10^{-5}$ for typical aperture diameters of 400 nm) is collected by a 0.5 NA, CaF₂ lens located behind the sample.

The samples sit on a metal disk that is supported on three piezoelectric transducers. [36] These piezoelectric elements are used to position the sample relative to the fixed near-field probe. The probe is mounted on a fourth piezoelectric transducer that is used in a shear-force detection circuit to position the tip a fixed distance from the surface. [37,38] The shear-force signal typically provides a topographic map of the surface although the adhesive forces acting between the probe and the PEA in this sample effectively precluded such a measurement.

Consequently, the spectral image data was collected with a nominal constant probe-sample separation (so-called constant height mode (CHM) imaging [39]) of 300 nm.

Following collection, the sample and reference beams are steered and focused onto the entrance slit of a 0.32 m monochromator containing a 75 groove/mm diffraction grating blazed at 4.5 μm . A 128 x 128 pixel InSb array detector is positioned at the focal plane of the monochromator to detect the horizontally dispersed reference and sample spectra, slightly offset from each other in the vertical direction. The method for calculating the normalized transmission spectra from the sample and reference line data is described in detail elsewhere. [12] The spectra recorded in parallel at each sample scan point were acquired in only two seconds, yielding an overall spectral image (50 x 50 spectra) acquisition time of approximately 1.5 hours.

The PS/PEA blend was prepared by mixing solutions of 4% PS ($M_w = 250,000$, Aldrich Company) and 4% PEA ($M_w = 119,300$, Aldrich Company) in toluene at a mass ratio of 30/70 and spin casting the solutions onto a precleaned glass cover slip at a speed of 2000 rpm for 30 s. FTIR transmission infrared spectra of the pure PEA and PS films were collected using a Nicolet 560x Fourier transform infrared spectrometer equipped with a mercury-cadmium-telluride (MCT) detector. The atomic force microscopy (AFM) image was recorded with a Dimension 3100 scanning probe microscope from Digital Instruments operated under ambient conditions using microfabricated silicon cantilever probes. [40]

Results and Discussion

Fig. 1(a) is an 8 x 8 μm tapping-mode, AFM image of the PS/PEA blend film displayed with a linear gray scale in which white is set to the maximum height (250 nm) and black is set to the minimum. On the basis of chemical modification/AFM measurements the raised domains

have been identified as being PS rich, with the matrix being PEA rich. [31] Note that the domain sizes range from approximately 200 nm to several micrometers. Fig. 1(b) is a schematic, 3D illustration of the likely morphology of this sample wherein spheroid inclusions (PS rich) of various sizes are distributed throughout a matrix phase (PEA rich) and the protruding portions of the inclusions can be correlated with the raised domains in the AFM image. Fig. 1(c) is an 8 x 8 μm unfiltered, near-field transmission CHM image of this sample acquired at a nominal wavelength of 3.36 μm (integrated over the spectral bandwidth of the laser), with a probe-sample separation of approximately 300 nm. The transmission contrast in this image (defined here as $T_{\text{max}} - T_{\text{min}} / T_{\text{max}}$) is 0.27 where white denotes the region of highest transmission and black the lowest and the pixel size is 80 nm. Note that the images shown in Fig. 1(a) and 1(c) are not of the same region of the sample as they were acquired on separate instruments. The near-field image shows several features of high transmission intensity that are presumably correlated with large (diameter > 1 μm) raised domains apparent in Fig. 1(a), while no features that might be correlated with the small domains distributed throughout the AFM image are apparent. This absence is due to some combination of the optical properties of the small domains and the large difference in the spatial resolution of AFM (< 50 nm) and aperture probe IR NSOM (300 – 500 nm). A topographic image acquired simultaneously with Fig. 1(c) would be quite useful in further cementing the connection between the domains seen in the AFM image and the regions of high transmission intensity in the near-field image; unfortunately due to the PEA tacticity this was not possible. Nevertheless, the sample analysis described in this paper assumes this correlation between the regions of high near-field transmission intensity and the raised circular domains seen in the AFM despite the lack of corresponding topographic data. Evaluation of ~ 15 near-field transmission images of various sections of this sample consistently indicates that

the regions of low transmission are spatially continuous while the high transmission regions are bounded circular features, thus reinforcing the validity of the postulated correlation.

The challenge in the analysis of this sample with IR NSOM is to exploit the distinct infrared optical properties of PS and PEA to extract information about the spatial distribution of these components on the sub-micrometer length scale. Note that this type of chemical information is difficult to extract from atomic force measurements; previous efforts were successful only in conjunction with the selective chemical modification of one of the phases (hydrolytic acid etching of PEA). [31] Fig. 2 shows the FTIR absorbance spectra of a 2 μm thick pure PS film (solid line) and a pure PEA thin film (dashed line) in the CH stretching region. The PEA spectrum has been scaled to show peak absorbance equal to that of PS, to facilitate visual comparison. There are obvious differences in this spectral region that offer the opportunity to distinguish between these two materials, including distinct bands of PS absorbance (3025 cm^{-1}), and PEA absorbance (2980 cm^{-1}). The shaded gray region in Fig. 2 represents the relative intensity spectrum of the broadband infrared laser tuned to the center wavelength ($\lambda = 3.36\text{ }\mu\text{m}$) used to acquire the near-field spectral images described in this paper. (Note that the slight asymmetry in the laser spectrum often results from alignment of the laser for an optimal combination of power and bandwidth.) The sharp edges of the spectrum at 2835 cm^{-1} and 3050 cm^{-1} occur where the dispersed light falls off the edges of the array detector. It is worth noting that the S/N ratio varies considerably across the spectrum, as the photon flux onto the edge pixels is nominally an order of magnitude less than the flux onto the center pixels. Use of this center wavelength yields near-field spectral image frames across the laser spectrum including those at 2922 cm^{-1} (PS/PEA absorbance), 2980 cm^{-1} (peak PEA absorbance) and 3025 cm^{-1} (peak PS absorbance). It is a measure of the power of broadband IR NSOM that these three image frames

alone can be expected to provide significant information on the spatial distribution of the PS and PEA components.

The real parts of the refractive indices for these two materials are, in all likelihood, quite different at this wavelength. They differ by $\Delta n(n_{\text{PS}}-n_{\text{PEA}}) = 0.12$ at the sodium D line at 589 nm; [41] Δn at 3.36 μm is presumably similar. It is also worth noting that the refractive indices of both polymers vary somewhat over the spectral range shown in Fig. 2 as the absorption resonances give rise to dispersive features in n via the Kramers-Kronig relations. [42] n_{PS} is known to vary by $\Delta n = 0.024$ over this spectral range. [43] Because near-field transmission data truly reflect spatial variations in extinction (with scattering and absorption components), image interpretation requires consideration of not only the distinct absorption spectra of these two materials but scattering effects as well.

Fig. 3 is a set of near-field transmission images, simultaneously acquired at 2922 cm^{-1} (a), 2980 cm^{-1} (b) and 3025 cm^{-1} (c). (Note that these images are extracted from the same data set that was integrated over frequency to produce Fig. 1(c).) The transmission contrast in these images is 0.28, 0.27 and 0.23, respectively (each displayed with an independent linear gray scale). The immediately obvious conclusion is that, while there are small differences in these images, the source of the majority of the image contrast is independent of frequency, despite the large differences in absorption over this spectral range. Recall that the both PS and PEA absorb at 2922 cm^{-1} , 2980 cm^{-1} is a distinct PEA absorbance peak, and that 3025 cm^{-1} is a distinct PS absorbance peak. This suggests that, at least for this sample, absorption is not the dominant source of near-field image contrast in the C-H stretching region. Scattering effects due to the sample topology and to the variation in the real refractive indices of the sample components appear to be the dominant source of contrast. In the context of IR NSOM, the influence of

sample topology and real refractive index on the scattering of non-propagating evanescent waves into propagating modes is discussed in reference 13.

While inspection of spectral image frames corresponding to different frequencies is an effective tool for evaluation of broadband near-field data, it is perhaps more useful to look directly at the spectra corresponding to (x,y) scan points. A significant issue in looking at spectral data is the choice of background spectrum. Note that all of the spectra are normalized in real time to a reference (no sample) spectrum. This has the effect of largely removing the gaussian line shape and amplitude fluctuations of the laser (see Ref. 12 for further discussion of this normalization procedure). However, this process often results in a fixed pattern, baseline response that is sufficiently structured to obscure the identification of small variations in transmission. In these cases, it is useful to normalize the spectral response at each (x,y) scan point to some suitable background spectrum from the image, effectively removing the baseline structure and focusing on spatial variations in the spectral response with respect to the background spectrum. For this sample, the background spectrum was calculated by averaging over all (x,y) points except those of high transmission intensity. This choice was motivated by the assumed correlation between the high transmission intensity regions in the near-field images and the circular domains seen in the AFM images and the expectation that the spectra of these regions would differ from those of the rest of the sample. Note that eliminating the relatively small number of high transmission intensity pixels (largely composing the three bright circular regions seen in Fig. 1(c)) altered the average spectrum very little and analysis using an average spectrum computed with all pixels yields the same conclusions drawn with this choice of background spectrum.

Three representative, near-field transmission spectra are shown in Fig. 4 along with the far-field PS and PEA absorbance spectra. The transmission magnitudes are corrected by normalization to the aforementioned average background spectrum and the spatial points A, B, and C are identified in Fig. 1(c). These spectra reinforce the conclusions drawn from analysis of the spectral image frames in Fig. 3. The spectrum from point B (moderate integrated near-field transmission intensity) is very similar to the average spectrum and shows very little spectral structure. The point C spectrum (low integrated near-field transmission intensity) shows lower transmission consistently across the frequency range, again showing very little structure. The point A spectrum (high integrated near-field transmission intensity) shows a small degree of spectral structure (discussed below) but the increased transmission is generally independent of frequency. This is consistent with analysis of the spectral image frames, which suggest that the principal source of image contrast is nominally independent of frequency in this spectral range, and thus is clearly not absorption. The principal sources of extinction in these images are scattering effects related to the sample topography and to the difference between n_{PS} and n_{PEA} . It is difficult to distinguish these effects, particularly when they are correlated, as is likely the case here. While the obvious appeal of IR near-field imaging is the incorporation of specific molecular absorption resonances as a source of contrast, clearly interpretation of images such as these solely in terms of absorption is unfounded.

Extraction of information about the spatial variation in chemical composition for this sample requires a close inspection of the spectral data, as to first order the transmission contrast is independent of frequency. The spectra from points A, B, and C can easily be converted to absorbance spectra for comparison to the spectra of the component materials shown in Fig. 2. Note that the different average transmissions appear as baseline offsets in absorbance although

these can be removed for purposes of comparison by setting the absorbance at an off-resonance frequency (2880 cm^{-1}) to zero. This highlights the differences between absorption on and off resonance and removes the frequency independent baseline offsets that are due to scattering effects rather than absorption. Fig. 5 shows the absorbance spectra for points A (solid line) and C (dotted line); because the spectra from points B and C are very similar the point B spectrum is excluded. Also shown in dark gray is a PS absorbance spectrum, scaled to the intensity expected for a 500 nm thick film. The weak spectral structure seen at point A appears to match the absorbance spectrum of PS reasonably well, whereas there is no indication of absorption at point C. Note that the spatial point that corresponds to the largest absorption is also the point of largest integrated transmission (lowest extinction). This is possible because the absorption contribution to the transmission (extinction) contrast is quite small compared to the spatial variation in the scattering contribution. This surprising result points to the inherent difficulty in extracting information about spatial variations in infrared absorption, and consequently chemical composition, from single wavelength near-field images. This ability to distinguish between the absorption and scattering contributions to near-field extinction is a clear strength of broadband IR NSOM.

The absorbance magnitudes at 2922 cm^{-1} and 3025 cm^{-1} in the point A spectrum match those expected for a 500 nm thick PS film. Analysis of the sample with AFM scratch measurements suggests a continuum phase thickness of approximately 300 nm. Given an average circular domain feature height of 150-200 nm in the AFM images, a rough estimate of the inclusion depth based on AFM is in good agreement with an estimate of the PS layer depth extracted from the near-field infrared absorbance spectrum in Fig. 5. There are several issues regarding this interpretation of the near-field IR data that should be mentioned. The near-field

absorbance spectra reported here are differential and thus characterization of the inclusion thickness based on absorption assumes that there is an insignificant amount of PS distributed throughout the continuum phase. Clearly, the S/N ratio for the spectrum in Fig. 5 is relatively low and this sample presumably defines the upper limits of the instrumental sensitivity in this spectral region for polymers. Note also that the origin of the feature around 2970 cm^{-1} is uncertain although it occurs in a spectral region of PEA absorption. Finally, the expectation of similarity between the near-field spectra and the far-field absorbance spectra ignores potential band-shifting effects due to Kramers-Kronig variations in n around absorption resonances. [13] Nevertheless, a detailed analysis of the near-field spectral images does reveal absorbance spectra that are consistent with a sample structure consisting of nominally 500 nm thick PS rich inclusions distributed throughout a PEA matrix, as suggested by previous chemical modification/AFM measurements.

Conclusions

The application of broadband, near-field infrared microscopy to the analysis of a thin film PS/PEA blend has been described. The near-field transmission contrast in the C-H stretching region is dominated by scattering effects rather than by absorption. The capability of broadband IR NSOM in distinguishing between these effects is clearly demonstrated, as are the difficulties in interpreting single wavelength, infrared near-field images solely in terms of absorption. Analysis of the near-field absorbance spectra provides information about the chemical morphology of the sample that is consistent with earlier chemical modification/AFM studies. Ongoing challenges reside in the development of a more quantitative understanding of the factors dictating the near-field spectral response of complex, heterogeneous nanometer scale systems such as this polymer blend sample.

Acknowledgments

The authors thank J.A. Woolam for providing information regarding the variation of n_{PS} in the infrared.

References

- [1] E. H. Synge, *Phil. Mag.* 6 (1928) 356.
- [2] D. W. Pohl, W. Denk, and M. Lanz, *Appl. Phys. Lett.* 44 (1984) 651.
- [3] A. Lewis, M. Isaacson, A. Harootunian, and A. Muray, *Ultramicroscopy* 13 (1984) 227.
- [4] E. Betzig, P. L. Finn, and J. S. Weiner, *Appl. Phys. Lett.* 60 (1992) 2484.
- [5] R. Toledo-Crow, P. Yang, T. Chen, and M. Vaez-Iravani, 60 (1992) 2957.
- [6] A. Piednoir and F. Creuzet, *Micron* 27 (1996) 335.
- [7] R. Bachelot, P. Gleyzes, and A. C. Boccara, *Opt. Lett.* 20 (1995) 1924.
- [8] M. K. Hong, A. G. Jeung, N. V. Dokholyan, T. I. Smith, H. A. Schwettman, P. Huie, and S. Erramilli, *Nuc. Inst. Meth. Phys. Res. B* 144 (1998) 246.
- [9] B. Knoll and F. Keilmann, *Nature* 399 (1999) 134.
- [10] D. T. Schaafsma, R. Mossadegh, J. S. Sanghera, I. D. Aggarwal, M. Luce, R. Generosi, P. Perfetti, A. Cricenti, J. M. Gilligan, and N. H. Tolk, *Opt. Eng.* 38 (1999) 1381.
- [11] B. Dragnea, J. Preusser, W. Schade, S. R. Leone, and W. D. Hinsberg, *J. Appl. Phys.* 86 (1999) 2795.
- [12] C. A. Michaels, S. J. Stranick, L. J. Richter, and R. R. Cavanagh, *J. Appl. Phys.* 88 (2000) 4832.
- [13] D. V. Palanker, D. M. Simanovskii, P. Huie, and T. I. Smith, *J. Appl. Phys.* 88 (2000) 6808.
- [14] B. B. Akhremitchev, S. Pollack, and G. C. Walker, *Langmuir* 17 (2001) 2774.
- [15] S. Webster, D. N. Batchelder, and D. A. Smith, *Appl. Phys. Lett.* 72 (1998) 1478.
- [16] M. Goetz, D. Drews, D. R. T. Zahn, and R. Wannemacher, *J. Lumin.* 76-7 (1998) 306.
- [17] C. L. Jahncke, M. A. Paesler, and H. D. Hallen, *Appl. Phys. Lett.* 67 (1995) 2483.
- [18] R. M. Stöckle, V. Deckert, C. Fokas, D. Zeisel, and R. Zenobi, *Vib. Spec.* 22 (2000) 39.
- [19] S. R. Emory and S. M. Nie, *Anal. Chem.* 69 (1997) 2631.
- [20] C. E. Jordan, S. J. Stranick, R. R. Cavanagh, L. J. Richter, and D. B. Chase, *Surf. Sci.* 435 (1999) 48.
- [21] Y. Narita, T. Tadokoro, T. Ikeda, T. Saiki, S. Mononobe, and M. Ohtsu, *Appl. Spec.* 52 (1998) 1141.
- [22] N. Hayazawa, Y. Inouye, Z. Sekkat, and S. Kawata, *Opt. Commun.* 183 (2000) 333.
- [23] F. Keilmann, D. W. van der Weide, T. Eickelkamp, R. Merz, and D. Stöckle, *Opt. Commun.* 129 (1996) 15.
- [24] D. W. van der Weide and P. Neuzil, *J. Vac. Sci. Technol. B* 14 (1996) 4144.
- [25] C. Gao and X. D. Xiang, *Rev. Sci. Instrum.* 69 (1998) 3846.
- [26] D. E. Steinhauer, C. P. Vlahacos, F. C. Wellstood, S. M. Anlage, C. Canedy, R. Ramesh, A. Stanishevsky, and J. Melngailis, *Appl. Phys. Lett.* 75 (1999) 3180.
- [27] M. Abu-Teir, M. Golosovsky, D. Davidov, A. Frenkel, and H. Goldberger, *Rev. Sci. Instrum.* 72 (2001) 2073.
- [28] I. I. Smolyaninov, A. V. Zayats, and C. C. Davis, *Phys. Rev. B* 56 (1997) 9290.
- [29] S. I. Bozhevolnyi and T. Geisler, *J. Opt. Soc. Am. A* 15 (1998) 2156.
- [30] R. D. Schaller and R. J. Saykally, *Langmuir* 17 (2001) 2055.
- [31] D. Raghavan, X. Gu, T. Nguyen, and M. van Landingham, *J. Poly. Phys. B* 39 (2001) 1460.
- [32] P. Hoffmann, B. Dutoit, and R.-P. Salathé, *Ultramicroscopy* 61 (1995) 165.

- [33] R. Stöckle, C. Fokas, V. Deckert, R. Zenobi, B. Sick, B. Hecht, and U. P. Wild, *Appl. Phys. Lett.* 75 (1999) 160.
- [34] M. A. Unger, D. A. Kossakovski, R. Kongovi, J. L. Beauchamp, J. D. Baldeschwieler, and D. V. Palanker, *Rev. Sci. Instrum.* 69 (1998) 2988.
- [35] M. K. Reed and M. K. S. Shepard, *IEEE J. Quantum Electron.* 32 (1996) 1273.
- [36] K. Besocke, *Surf. Sci.* 181 (1987) 145.
- [37] J. Barenz, O. Hollricher, and O. Marti, *Rev. Sci. Instrum.* 67 (1996) 1912.
- [38] S. J. Stranick, L. J. Ritcher, and R. R. Cavanagh, *J. Vac. Sci. Technol. B* 16 (1998) 1948.
- [39] B. Hecht, H. Bielefeldt, Y. Inouye, D. W. Pohl, and L. Novotny, *J. Appl. Phys.* 81 (1997) 2492.
- [40] Certain commercial equipment, instruments, or materials are identified in this paper to specify adequately the experimental procedure. In no case does such identification imply recommendation or endorsement by the National Institute of Standards and Technology, nor does it imply that the materials or equipment identified are necessarily the best available for the purpose.
- [41] J. Brandrup, E. H. Immergut, and E. A. Grulke (Eds.), *Polymer Handbook*, John Wiley & Sons, New York, 1999.
- [42] C. F. Bohren and D. R. Huffman, *Absorption and Scattering of Light by Small Particles*, John Wiley & Sons, New York, 1983.
- [43] J. A. Woolam, personal communication.

Figure Captions

Figure 1. (a) 8 x 8 μm tapping-mode, AFM topographic image of a PS/PEA blend film displayed with a linear gray scale from black (minimum height) to white (250 nm). (b) Schematic illustration of the sample structure deduced from chemical modification/AFM measurements in which the spheroidal inclusions are PS rich and the matrix is PEA rich. (c) 8 x 8 μm near-field transmission CHM image of PS/PEA blend film acquired independently of (a) at $\lambda = 3.36 \mu\text{m}$ with a probe-sample separation of approximately 300 nm. A, B and C identify spatial points corresponding to spectra displayed in Fig. 4.

Figure 2. Scaled infrared absorbance spectra of PS (solid line) and PEA (dashed line) in the C-H stretching region along with the relative intensity spectrum of the broadband IR laser (dark gray) used to acquire near-field spectral images of the PS/PEA blend film.

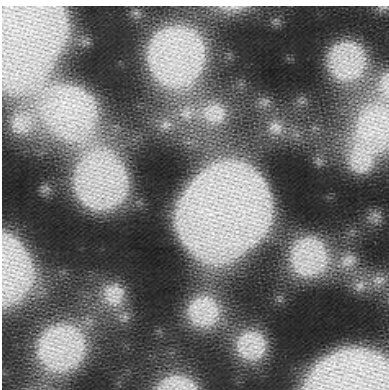
Figure 3. 8 x 8 μm near-field transmission spectral frames of the PS/PEA blend film simultaneously acquired at (a) 2922 cm^{-1} , (b) 2980 cm^{-1} , (c) 3025 cm^{-1} . These images are displayed using independent linear gray scales in which white is set to the highest transmission and black is set to the lowest.

Figure 4. Scaled infrared absorbance spectra (left axis) of PS (solid line) and PEA (dashed line) in the C-H stretching region along with normalized near-field transmission spectra (right axis) corresponding to the spatial points A, B, and C indicated in Fig. 1(c).

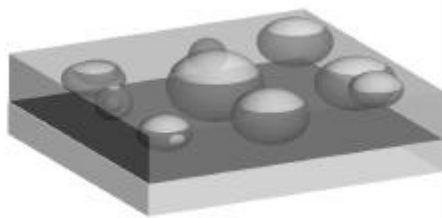
Figure 5. Scaled near-field infrared absorbance spectra corresponding to points A (solid line) and C (dotted line) indicated in Fig. 1(c) along with a scaled far-field infrared absorbance spectrum of PS (dark gray).

Figure 1 S.J. Stranick
Vib. Spec.

(a)



(b)



(c)

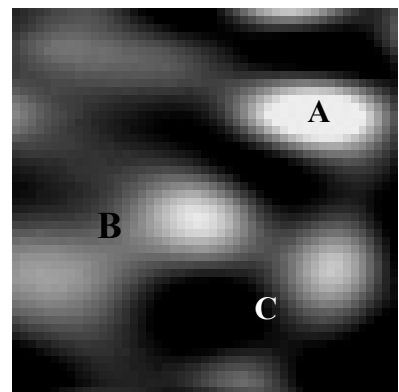


Figure 2 S.J. Stranick
Vib. Spec.

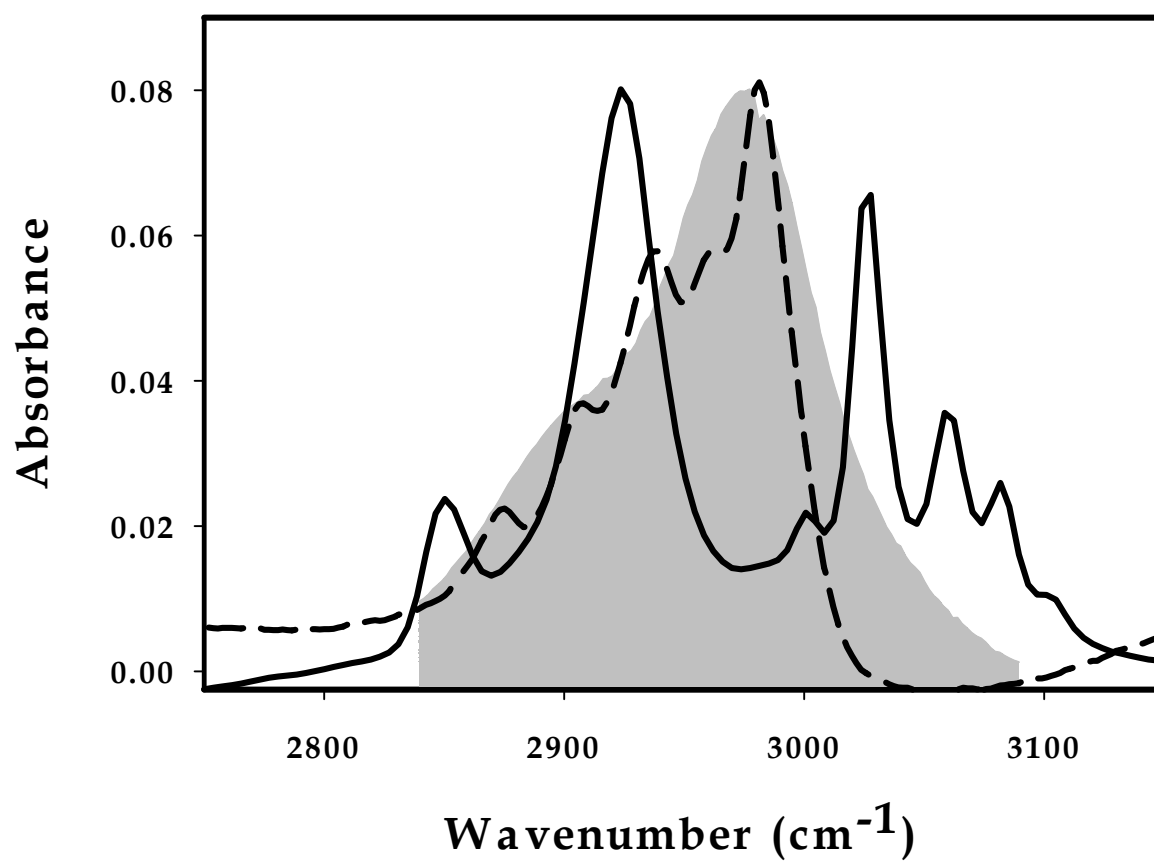


Figure 3 S.J. Stranick
Vib. Spec.

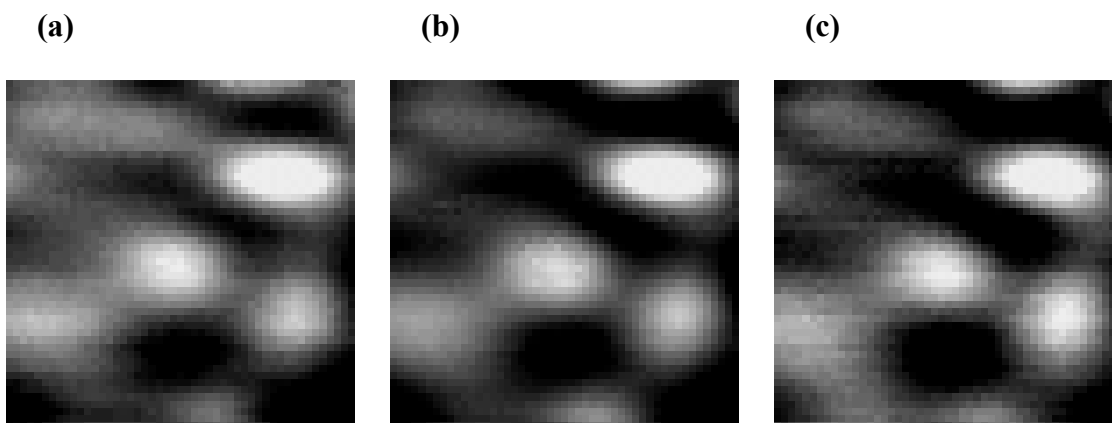


Figure 4 S.J. Stranick
Vib. Spec.

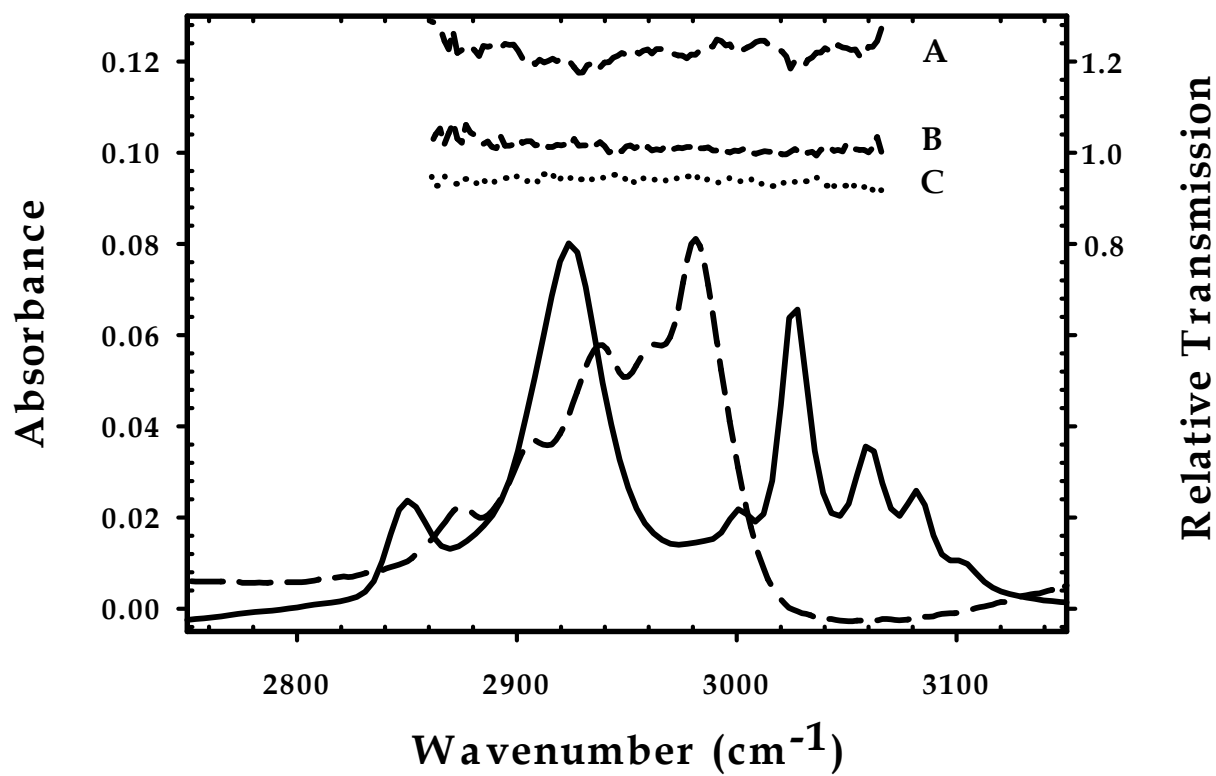


Figure 5 S.J. Stranick
Vib. Spec.

